

Online supplement for Tromp et al., Altered Uncinate Fasciculus Microstructure in Childhood Anxiety Disorders in Boys But Not Girls. Am J Psychiatry (doi: 10.1176/appi.ajp.2018.18040425)

## **CONTENTS**

### **Supplemental Methods**

**Figure S1. Anxiety symptom scores by group and sex**

**Figure S2. Hormones by group and sex**

**Table S1. Exploration of interactions on UF FA**

**Figure S3. UF FA as a function of age, split by sex**

**Figure S4. Tract statistics**

**Figure S5. Group differences in whole brain FA split by sex**

**Table S2. Cluster coordinates of group differences in whole brain FA split by sex**

**References**

## Supplemental Methods

**Participants:** Sixty-seven children (ages 8-12 years) were recruited from the Madison, WI area via clinician referral and through newspaper/e-mail advertisements. An additional 48 children and adolescents (ages 8-17 years) were recruited in collaboration with the National Institute of Mental Health (NIMH). Because of our interest in medication free, preadolescent children, 4 individuals were excluded due to previous medication use, and 13 were excluded because they were older than 12 years of age. Imaging data from some of the subjects was previously published<sup>1-5</sup>; none of these publications contained DTI data.

Cross-site fidelity of K-SADS-PL was maintained using procedures employed in prior studies. This involved a series of meetings between clinicians at the two sites and a reliability study, whereby 26 tapes of interviews from the UW site were reviewed by a Board-Certified child psychiatrist (DSP) from the NIMH site. This revealed high levels of diagnostic agreement, where both clinicians reached total agreement on child anxiety diagnosis in all 26 cases. Fifty-two participants (51.9% girls) received a current diagnosis of at least one of the following diagnoses based on DSM-IV: generalized anxiety disorder, separation anxiety disorder, social anxiety disorder or anxiety disorder not otherwise specified. As expected in a sample of this age group with ADs<sup>6,7</sup>, a majority of the patients presented with comorbid conditions, including at least one other anxiety disorder (n = 30), attention deficit hyperactivity disorder (ADHD; n = 6), oppositional defiant disorder (ODD; n = 6), or major depressive disorder (MDD; n = 3).

Beyond diagnosis, children's symptoms were rated by both the child and a parent using the Screen for Child Anxiety and Related Emotional Disorders (SCARED; 4 parent and 3 child ratings missing)<sup>8</sup>. Depressive symptoms were assessed by children's self-ratings on the Child Depression Inventory (CDI; 1 missing)<sup>9</sup>. Externalizing behaviors were assessed by parents using the Conners' Parent Rating Scale-Revised (CPRS-R; 9 missing)<sup>10</sup>. Child IQ was evaluated using the Weschler Abbreviated Scale of Intelligence (WASI-II, 2011, Full Scale IQ-2; 2 missing)<sup>11</sup>, and physical development was rated using the Tanner stages (6 missing)<sup>12</sup>.

Exclusion criteria for UW included current or past obsessive-compulsive disorder, post-traumatic stress disorder, autism spectrum disorder, bipolar disorder,

schizophrenia, an IQ below 80, as well as major medical illnesses. NIMH exclusion criteria included current MDD, obsessive-compulsive disorder, and posttraumatic stress, as well as a lifetime history of psychosis, bipolar disorder, or extreme trauma.

**DTI acquisition:** At both sites brain images were collected on a 3.0 Tesla GE MR750 scanner (GE Healthcare; Waukesha, WI). At the UW site an 8-channel head coil was used, while NIMH used a 32-channel head coil. At both sites diffusion-weighted MRI scans were obtained using a two-dimensional echo planar imaging diffusion-weighted spin-echo sequence (TR = 6500 ms, TE = 62.2 ms, flip angle = 90 degrees, matrix = 128 x 128 interpolated to 256 x 256, FOV = 256 mm, 2.9 mm contiguous slices, echo-planar echo spacing = 568  $\mu$ s, b-value of 1000 s/mm<sup>2</sup>, 48 optimal non-collinear directions and 8 non-diffusion-weighted images). Structural and functional MRI scans were collected during the same scan session but are not reported here<sup>1-5</sup>. Before scanning, children completed a mock MRI session, which has been shown to reduce movement in pediatric neuroimaging studies<sup>13</sup>.

**Steroid hormone collection:** Because of the unique nature of this pre-adolescent sample, we wanted to be sure that observed effects could not be accounted for by differences in steroid hormone levels. Thus, saliva samples for hormone analyses were collected at three time points from a subset of subjects recruited at the UW site. In total 60 (36 AD, 24 control) subjects had saliva samples taken. The first sample was collected at the beginning of the study visit, the second one was collected halfway through the MRI scans (approximately 90 minutes later), and the last sample took place immediately following the final MRI scan (~45 minutes after the second sample). Subjects were instructed to refrain from eating for 1 hour before sample collection began. Participants salivated into a tube using a straw to collect a 1.5 ml sample at each time point.

**DTI analyses:** The diffusion-weighted volumes from each individual were transformed into a 3-dimensional diffusion tensor for each voxel in the brain using the following procedures. Although there were no significant differences in estimated motion between

our healthy controls (mean Euclidian distance:  $0.760 \pm 0.630\text{mm}$ ) and AD children (mean Euclidean distance:  $0.710 \pm 0.337\text{mm}$ ) ( $t(92) = 0.571$ ,  $p = 0.570$ ), distortions due to head motion and eddy currents were corrected using FSL's tools for rigid registration. The gradient direction matrix was corrected for the applied rotations after rigid registration<sup>14</sup>. Since samples that include young or clinical populations can suffer from reduced image quality due to smaller head size or other causes, a robust estimation of tensors by outlier rejection (RESTORE, as implemented in Camino software)<sup>15</sup> was used to minimize the influence of all sources of noise on the tensor calculation. This method uses an average noise estimation to determine which diffusion measurements are outliers and excludes those from the tensor computation, and has been shown to increase reliability of the tensor estimation in clinical populations<sup>16</sup>. The resulting DTI scans contain 3 major vectors for each voxel in the brain that model water diffusion as shaped by local microstructure.

In order to compare diffusion measures across subjects all individuals were normalized to a study-specific template space that was then warped to MNI152-space, to produce each subject's MNI-space tensor-map. We used a high-dimensional registration method that incorporates the tensor orientation (DTI-TK)<sup>17</sup>, to make optimal use of the additional information available in DTI scans. This method outperforms intensity based normalization of diffusion images and shows improved white matter shape and architecture representation<sup>18,19</sup>. The final population template was constructed after multiple registration iterations and then aligned to the 1 mm isotropic MNI152-template; this warp was then applied to all normalized images. All images were smoothed with a 4-mm full width at half maximum (FWHM) kernel.

To allow for characterization and quantification of the structural properties of the tissue as measured with diffusion imaging, we extracted four diffusion measures. Fractional anisotropy (FA) is a measure that assesses the relative variability of the diffusion as a function of direction, allowing for selective sensitivity to longitudinal diffusion. FA is highest in areas with highly organized white matter fiber pathways, and is taken to be a sensitive metric of the micro-structural integrity of these pathways<sup>20</sup>. Mean diffusivity (MD) is an average of all three main diffusion vectors and is sensitive to

the density of microstructure within each voxel. Axial diffusivity (XD) and radial diffusivity (RD) reflect the amount of longitudinal and transverse diffusion, respectively.

The population template created from all subjects was used for deterministic fiber tractography to delineate tracts of interest. Whole-brain fiber tracking was performed on the population template using Camino software<sup>15</sup> that implemented a fourth-order Runge-Kutta method combined with a tensor deflection (TEND) algorithm for optimal estimation of the fiber tracking directions<sup>21,22</sup>. Fiber tracking was terminated in voxels where FA was below 0.1 or where the angle between consecutive streamline steps was more than 90 degrees. Seven fiber pathways were iteratively delineated in template space using anatomically defined waypoints<sup>23–27</sup>, using a 3D tract visualization program (trackvis.org). Tracts of interest included cortico-limbic association pathways previously implicated in ADs, such as UF<sup>28–33</sup>, cingulum bundle (CING)<sup>32,34</sup>, superior longitudinal fasciculus (SLF)<sup>31–33</sup>, fornix (FX)<sup>32</sup>, and inferior frontal occipital fasciculus (IFO)<sup>32,33</sup>. Tracts shown to have anxiety-related changes in other publications were also extracted, including thalamocortical projection fibers in the internal capsule (IC)<sup>32,33</sup>, and interhemispheric commissural fibers of the corpus callosum (CC)<sup>35</sup>.

Next, in order to quantify the microstructure of an entire white matter structure a weighted mean was calculated per tract for each diffusion measure per subject. The weighted mean of a tract (e.g. UF, CING, etc.) was calculated by first creating a scalar image of the number of fibers in the tract passing through each voxel as a proportion of the total number of fibers in that tract. We then multiplied this weighting factor by the value of the diffusion measure in that voxel (e.g. FA, MD, etc.), and averaged that to get the mean weighted scalar value for each tract<sup>36</sup>. This approach allows for the differential weighting of voxels that have a higher fiber count, which is most frequently observed in areas more central to the white matter tract of interest. Importantly, tract based analyses are able to pick up on pervasive yet subtle differences that are distributed across the length of a tract, an attribute that may be missed using conventional voxel-based methods. Thus, this method is well suited to identify tract-based differences for which alterations at any point in the tract might alter the efficacy of communication across the length of this pathway.

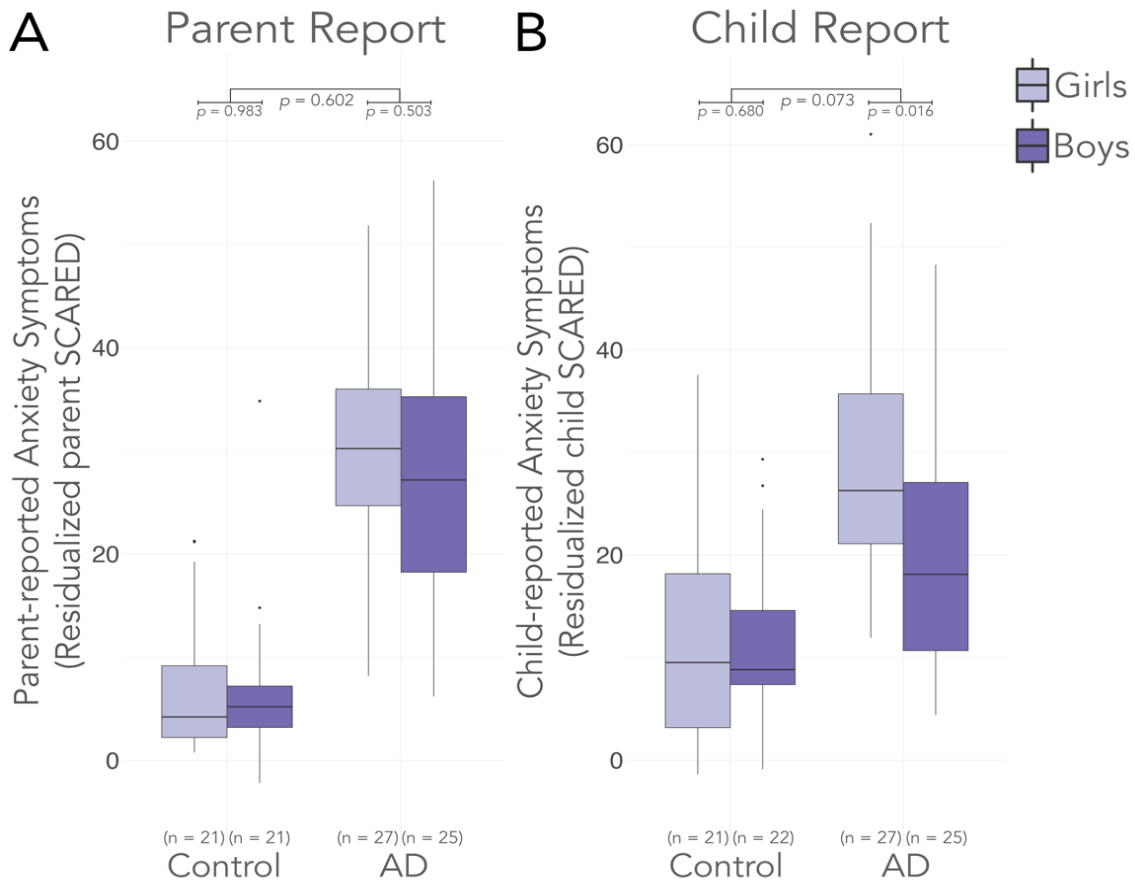
To explore potential anxiety-related white matter differences beyond the *a priori* determined regions in the tract-based analysis, voxel-based analysis of FA was performed across the whole brain. Group differences in whole brain FA, as well as an estimate of the interaction between group and sex on FA were estimated with a general linear model using permutation methods. This method makes fewer assumptions about the distribution of the underlying data and thus provides a more robust technique of making statistical inferences with regard to the assumed statistical significance<sup>37</sup>. Analyses included age, sex and site as covariates and were run using FSL's randomise tool<sup>38</sup>. To control the family-wise error rate a threshold-free cluster enhancement (TFCE) was applied on the voxel-wise statistics<sup>39</sup>.

**Steroid hormone analyses:** Cortisol, testosterone and estradiol levels were measured in separate enzyme immunoassays using kits purchased from Salimetrics (State College, PA). Prior to each assay, saliva was thawed and spun at 1,500 x g for 15 min at room temperature to remove particulate. The supernatant was assayed in duplicate following manufacturer's instructions. Samples that had assay results with CV% > 20 were repeated. The inter-assay CV% was determined using the high and low standards provided by the kits. For cortisol, the inter-assay CV% was 3.4 at 0.99 µg/dl and 2.6 at 0.11 µg/dL; for testosterone, the inter-assay CV% was 4.8 at 219.5 pg/ml and 13.0 at 22.0 pg/ml; for estradiol, the inter-assay CV% was 6.4 at 16.9 pg/ml and 2.3 at 7.1 pg/ml. For two individuals, all samples were excluded due to saliva that was too viscous to pipet. Two other samples were excluded because they either had inter-assay CV above the 20% cutoff, or were 5 standard deviations outside of the mean.

All hormone measures were residualized for time of day across the whole sample. Statistical analyses for these hormones were all run with robust linear regression models in order to mitigate the effect of outliers on the results. Models were run using the statsmodels package in Python<sup>40</sup>. Repeated measures ANOVA analyses indicated no significant group by time interactions for any hormone ( $p > 0.14$ ), so the values of the three time points were averaged into one mean for subsequent analyses.

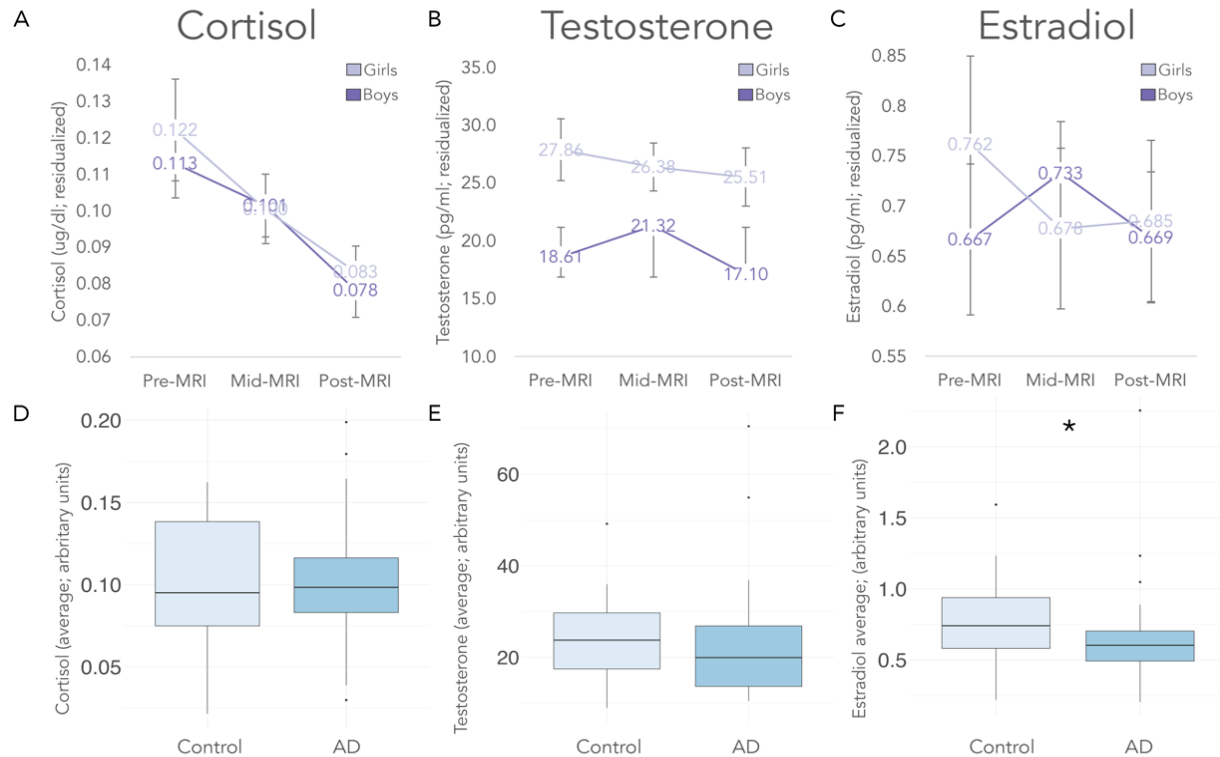
### FIGURE S1. Anxiety symptom scores by group and sex

Box-plot of A) parent reported and B) child reported symptoms of anxiety (SCARED) scores, split by group and sex. Girls in light purple, boys in dark purple. SCARED scores are residualized for age and site.



## FIGURE S2. Hormones by group and sex

Line graph of the progression of average steroid hormone levels A) Cortisol, B) Testosterone, and C) Estradiol, as measured across three time points (pre-MRI, mid-MRI, post-MRI), for each sex (girls in light purple, boys in dark purple). Error bars indicate standard error of the mean. Repeated measures ANOVA indicated that only cortisol levels significantly changed over time ( $p = 0.006$ ). There were no significant group by time interactions for any hormone ( $p_s > 0.14$ ). Thus, for subsequent analyses the hormone values were averaged across time. Box-plots by group are shown for D) Cortisol, E) Testosterone, and F) Estradiol. Group differences were only significant for estradiol ( $p = 0.037$ ). All measures were residualized for time of day.





**TABLE S1. Exploration of interactions on UF FA**

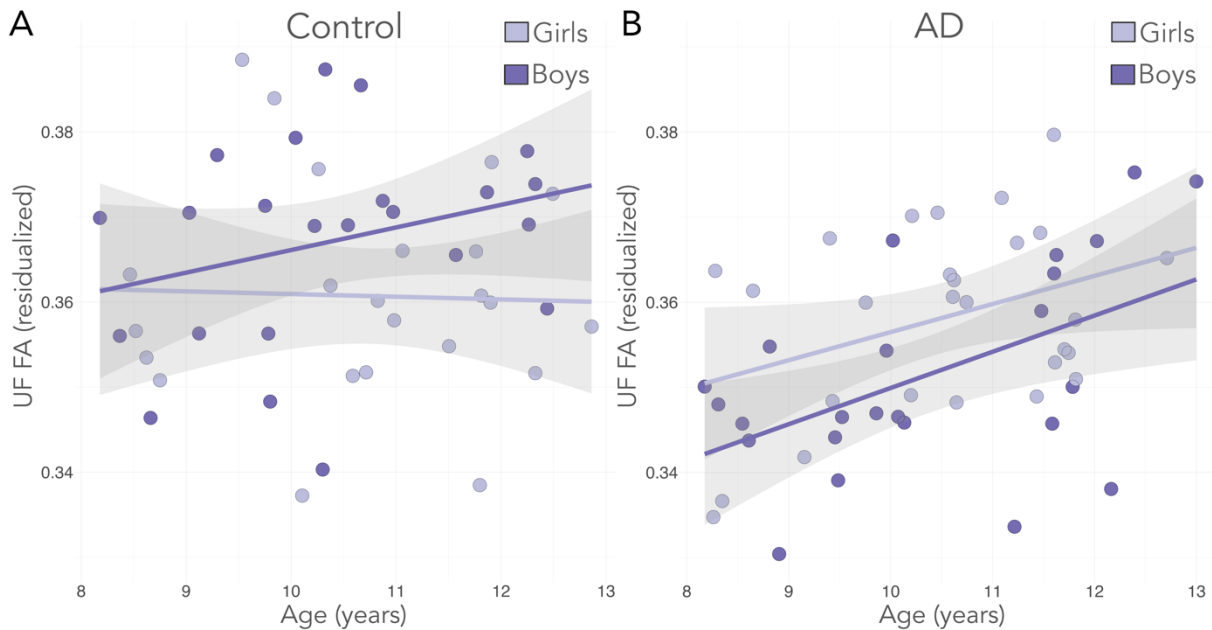
Significance of robust regression of demographics, symptoms and endocrine measures on uncinate fasciculus (UF) fractional anisotropy (FA). Values reported are *p*-values. Degrees of freedom (df) are noted.

UF FA ~ Group + Sex + Age + Group*Sex + Group*Age + Sex*Age + Group*Sex*Age (+ Site)					
Demographic		Demographic	Group*Demographic	Sex*Demographic	Group*Sex*Demographic
(df = 89)	Group	<0.001*			
(df = 89)	Sex	0.832	0.007*		
(df = 89)	Age	0.008*	0.253	0.324	0.849
UF FA ~ Symptom + Group*Symptom + Sex*Symptom + Group*Sex*Symptom (+ Group + Sex + Age + Group*Sex)					
Symptom		Symptom	Group*Symptom	Sex*Symptom	Group*Sex*Symptom
(df = 77)	parent SCARED	0.711	0.779	0.295	0.375
(df = 78)	child SCARED	0.832	0.924	0.573	0.461
(df = 87)	Depression (CDI)	0.814	0.947	0.967	0.447
(df = 79)	ADHD (CPRS-R)	0.248	0.668	0.400	0.602
UF FA ~ Endocrine + Group* Endocrine + Sex* Endocrine + Group*Sex* Endocrine (+ Group + Sex + Age + Group*Sex)					
Endocrine		Endocrine	Group*Endocrine	Sex*Endocrine	Group*Sex*Endocrine
(df = 44)	Cortisol	0.885	0.958	0.064	0.745
(df = 44)	Testosterone	0.162	0.19	0.443	0.175
(df = 44)	Estradiol	0.526	0.276	0.873	0.283

\* indicates two-tailed significance

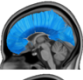
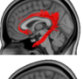
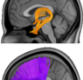
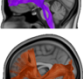
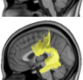

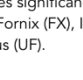
**FIGURE S3. UF FA as a function of age, split by group and sex**

Scatterplot of uncinate fasciculus (UF) fractional anisotropy (FA) plotted against age, graphs are split by group A) Control and B) anxiety disorder (AD). Slope lines and confidence intervals were drawn separately for girls (light purple) and boys (dark purple). UF FA scores are residualized for site.



### FIGURE S4. Tract statistics

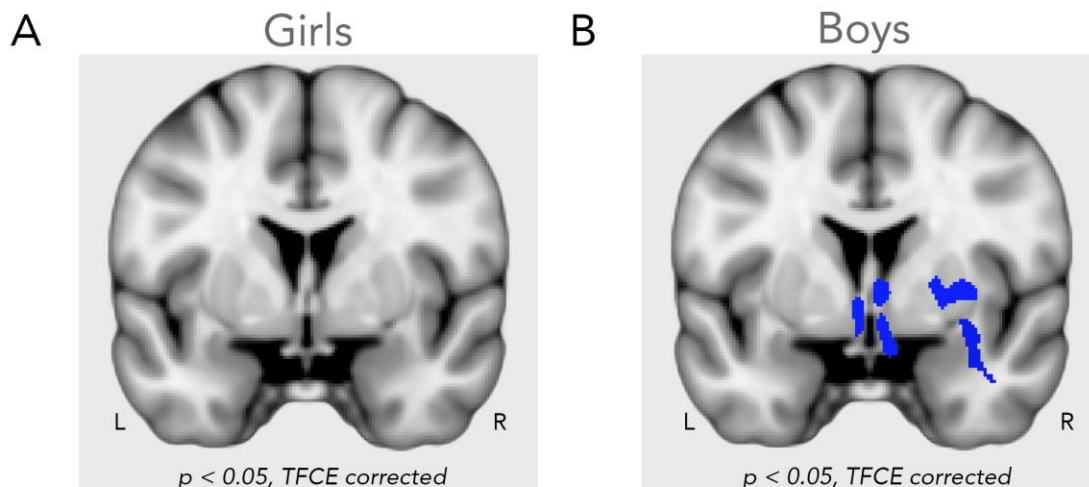
Weighted mean of mean diffusivity (MD), axial diffusivity (XD) and radial diffusivity (RD) by tracts for control and anxiety disorder (AD) subjects, with standard deviations in parentheses. Significance of the regression statistics for the main effect of group, as well as the interaction of group by sex are noted. All analyses include age, sex and site as covariates.

Bilateral WM Tract	MD		Group		XD		Group		RD		Group	
	Control	AD	p-values	p-values	Control	AD	p-values	p-values	Control	AD	p-values	p-values
CC 	0.793 (0.021)	0.802 (0.028)	0.160	0.218	1.274 (0.02)	1.277 (0.026)	0.844	0.387	0.552 (0.023)	0.565 (0.03)	0.068	0.191
CING 	0.792 (0.022)	0.797 (0.022)	0.604	0.053	1.033 (0.025)	1.033 (0.025)	0.404	0.327	0.671 (0.023)	0.68 (0.024)	0.231	0.029*
FX 	0.956 (0.058)	0.949 (0.061)	0.286	0.900	1.291 (0.067)	1.275 (0.072)	0.139	0.499	0.789 (0.056)	0.786 (0.057)	0.437	0.820
IC 	0.742 (0.027)	0.754 (0.027)	0.026*	0.046*	1.138 (0.038)	1.155 (0.039)	0.018*	0.101	0.544 (0.023)	0.554 (0.023)	0.049*	0.031*
IFO 	0.79 (0.019)	0.794 (0.021)	0.509	0.057	1.172 (0.026)	1.172 (0.025)	0.792	0.717	0.599 (0.022)	0.604 (0.024)	0.464	0.020*
SLF 	0.756 (0.023)	0.762 (0.023)	0.366	0.365	1.075 (0.026)	1.075 (0.023)	0.895	0.854	0.597 (0.024)	0.605 (0.028)	0.256	0.196
UF 	0.792 (0.016)	0.799 (0.016)	0.076	0.343	1.122 (0.022)	1.122 (0.021)	0.751	0.339	0.628 (0.017)	0.638 (0.017)	<b>0.006**</b>	0.047*

\* indicates significance at uncorrected levels, \*\* indicates significant results at Šidák corrected levels. Abbreviations: Corpus Callosum (CC), Cingulum bundle (CING), Fornix (FX), Internal Capsule (IC), Inferior Fronto-Occipital fasciculus (IFO), Stria Terminalis (STRIA), Superior Longitudinal Fasciculus (SLF), Uncinate Fasciculus (UF).

### FIGURE S5. Group differences in whole brain FA split by sex

Whole-brain voxel-wise results for group differences in fractional anisotropy (FA) for A) girls and B) boys separately, results are TFCE corrected. A) Results indicated that no clusters passed multiple comparison correction for girls, signifying there were no significant voxel-wise differences in FA values for girls with anxiety disorders (ADs) compared to healthy control girls ( $p > 0.05$ , TFCE corrected). However, boys did display significant group differences in voxel-wise FA levels between AD and healthy controls ( $p < 0.05$ , TFCE corrected, **eTable 2**, <https://neurovault.org/collections/161/>), Of the significant regions in the boys, most overlap with the results observed in the across sex analysis.



**TABLE S2. Cluster coordinates of group differences in whole brain FA split by sex**

Group differences in voxel-based analyses of whole-brain fractional anisotropy (FA) values for boys and girls separately. Overview of size and location of significant clusters after TFCE correction. There were no significant (n.s.) clusters for the girls.

Cluster #	Volume (mm <sup>3</sup> )	Location	Hemi-sphere	Peak t-value	Peak MNI Coordinate
<b>Boys</b>					
1	12922	CC/UF	L & R	5.99	( 88 153 73)
2	382	UF	R	3.82	(121 129 63)
3	113	SLF	R	5.70	(157 103 70)
4	108	IC	R	5.76	(102 100 141)
5	67	IFO/UF	L	4.28	(70 143 61)
6	55	CC/UF	L	5.41	(87 181 49)
7	29	IFO/IC	R	3.20	(116 145 106)
<b>Girls</b>					
n.s.					

Abbreviations: Corpus Callosum (CC), Internal Capsule (IC), Inferior Fronto-Occipital fasciculus (IFO), Superior Longitudinal Fasciculus (SLF), Uncinate Fasciculus (UF).

## References

1. Williams LE, Oler J a, Fox AS, et al. Fear of the Unknown: Uncertain Anticipation Reveals Amygdala Alterations in Childhood Anxiety Disorders. *Neuropsychopharmacology*. 2014;1-8. doi:10.1038/npp.2014.328.
2. Birn RM, Shackman AJ, Oler JA, et al. Evolutionarily conserved prefrontal-amygdalar dysfunction in early-life anxiety. *Mol Psychiatry*. 2014;19(January):915-922. doi:10.1038/mp.2014.46.
3. Gold AL, Steuber ER, White LK, et al. Cortical thickness and subcortical gray matter volume in pediatric anxiety disorders. *Neuropsychopharmacology*. 2017;42(12):2423-2433. doi:10.1038/npp.2017.83.
4. White LK, Sequeira S, Britton JC, et al. Complementary features of attention bias modification therapy and cognitive-behavioral therapy in pediatric anxiety disorders. *Am J Psychiatry*. 2017;174(8):775-784. doi:10.1176/appi.ajp.2017.16070847.
5. Gold AL, Brotman MA, Adleman NE, et al. Comparing Brain Morphometry Across Multiple Childhood Psychiatric Disorders. In: *Journal of the American Academy of Child and Adolescent Psychiatry*. Vol 55. ; 2016:1027-1037.e3. doi:10.1016/j.jaac.2016.08.008.
6. Kendall PC, Compton SN, Walkup JT, et al. Clinical characteristics of anxiety disordered youth. *J Anxiety Disord*. 2010;24(3):360-365. doi:10.1016/j.janxdis.2010.01.009.
7. Leyfer O, Gallo KP, Cooper-Vince C, Pincus DB. Patterns and predictors of comorbidity of DSM-IV anxiety disorders in a clinical sample of children and adolescents. *J Anxiety Disord*. 2013;27(3):306-311. doi:10.1016/j.janxdis.2013.01.010.
8. Birmaher B, Brent DA, Chiappetta L, Bridge J, Monga S, Baugher M. Psychometric properties of the Screen for Child Anxiety Related Emotional Disorders (SCARED): a replication study. *J Am Acad Child Adolesc Psychiatry*. 1999;38(10):1230-1236. doi:10.1097/00004583-199910000-00011.
9. Kovacs M. The Children's Depression, Inventory (CDI). *Psychopharmacol Bull*. 1985;21(4):995-998.
10. Conners CK, Sitarenios G, Parker JD, Epstein JN. The revised Conners' Parent Rating Scale (CPRS-R): factor structure, reliability, and criterion validity. *J Abnorm Child Psychol*. 1998;26(4):257-268.
11. Wechsler D. WASI -II Wechsler abbreviated scale of intelligence -- second edition. 2011.
12. Morris NM, Udry JR. Validation of a self-administered instrument to assess stage of adolescent development. *J Youth Adolesc*. 1980;9(3):271-280. doi:10.1007/BF02088471.
13. de Bie HMA, Boersma M, Wattjes MP, et al. Preparing children with a mock scanner training protocol results in high quality structural and functional MRI scans. *Eur J Pediatr*. 2010;169(9):1079-1085. doi:10.1007/s00431-010-1181-z.
14. Leemans A, Jones DK. The B-matrix must be rotated when correcting for subject motion in DTI data. *Magn Reson Med*. 2009;61:1336-1349. doi:10.1002/mrm.21890.

15. Cook PA, Bai Y, Seunarine KK, Hall MG, Parker GJ, Alexander DC. Camino : Open-Source Diffusion-MRI Reconstruction and Processing. 2006;14:22858.
16. Chang L-C, Jones DK, Pierpaoli C. RESTORE: Robust estimation of tensors by outlier rejection. *Magn Reson Med*. 2005;53(5):1088-1095. doi:10.1002/mrm.20426.
17. Zhang H, Yushkevich PA, Alexander DC, Gee JC. Deformable registration of diffusion tensor MR images with explicit orientation optimization. *Med Image Anal*. 2006;10(5):764-785. doi:10.1016/j.media.2006.06.004.
18. Zhang H, Avants BB, Yushkevich PA, et al. High-dimensional spatial normalization of diffusion tensor images improves the detection of white matter differences: an example study using amyotrophic lateral sclerosis. *IEEE Trans Med Imaging*. 2007;26(11):1585-1597. doi:10.1109/TMI.2007.906784.
19. Adluru N, Zhang H, Fox AS, et al. A diffusion tensor brain template for rhesus macaques. *Neuroimage*. 2012;59(1):306-318. doi:10.1016/j.neuroimage.2011.07.029.
20. Alexander AL, Hurley SA, Samsonov AA, et al. Characterization of Cerebral White Matter Properties Using Quantitative Magnetic Resonance Imaging Stains. *Brain Connect*. 2011;1(6). doi:10.1089/brain.2011.0071.
21. Basser PJ, Pajevic S, Pierpaoli C, Duda J, Aldroubi A. In vivo fiber tractography using DT-MRI data. *Magn Reson Med*. 2000;44:625-632. doi:10.1002/1522-2594(200010)44:4<625::AID-MRM17>3.0.CO;2-O.
22. Lazar M, Weinstein DM, Tsuruda JS, et al. White matter tractography using diffusion tensor deflection. *Hum Brain Mapp*. 2003;18(4):306-321. doi:10.1002/hbm.10102.
23. Catani M, Howard RJ, Pajevic S, Jones DK. Virtual in Vivo Interactive Dissection of White Matter Fasciculi in the Human Brain. *Neuroimage*. 2002;17(1):77-94. doi:10.1006/nimg.2002.1136.
24. Catani M, Thiebaut M, Schotten D, Thiebaut de Schotten M. A diffusion tensor imaging tractography atlas for virtual in vivo dissections. *Cortex*. 2008;44(8):1105-1132. doi:10.1016/j.cortex.2008.05.004.
25. Mori S, Kaufmann WE, Davatzikos C, et al. Imaging Cortical Association Tracts in the Human Brain Using Diffusion-Tensor-Based Axonal Tracking. 2002;223:215-223. doi:10.1002/mrm.10074.
26. Wakana S, Jiang H, Nagae-Poetscher LM, van Zijl PCM, Mori S. Fiber tract-based atlas of human white matter anatomy. *Radiology*. 2004;230(1):77-87. doi:10.1148/radiol.2301021640.
27. Tromp D. DTI Tutorial 3 - Fiber Tractography. *doi.org*. February 2016. doi:10.15200/winn.146228.88526.
28. Phan KL, Orlichenko A, Boyd E, et al. Preliminary evidence of white matter abnormality in the uncinate fasciculus in generalized social anxiety disorder. *Biol Psychiatry*. 2009;66(7):691-694. doi:10.1016/j.biopsych.2009.02.028.
29. Baur V, Brühl AB, Herwig U, et al. Evidence of frontotemporal structural hypoconnectivity in social anxiety disorder: A quantitative fiber tractography study. *Hum Brain Mapp*. 2013;0(July):437-446. doi:10.1002/hbm.21447.
30. Hettema JM, Kettenmann B, Ahluwalia V, et al. Pilot multimodal twin imaging study of generalized anxiety disorder. *Depress Anxiety*. 2012;29(3):202-209.

- doi:10.1002/da.20901.
31. Baur V, Hänggi J, Rufer M, et al. White matter alterations in social anxiety disorder. *J Psychiatr Res*. 2011;45(10):1366-1372. doi:10.1016/j.jpsychires.2011.05.007.
  32. Tromp DPM, Grupe DW, Oathes DJ, et al. Reduced structural connectivity of a major frontolimbic pathway in generalized anxiety disorder. *Arch Gen Psychiatry*. 2012;69(9):925-934. doi:10.1001/archgenpsychiatry.2011.2178.
  33. Liao M, Yang F, Zhang Y, He Z, Su L, Li L. White matter abnormalities in adolescents with generalized anxiety disorder: a diffusion tensor imaging study. *BMC Psychiatry*. 2014;14(1):41. doi:10.1186/1471-244X-14-41.
  34. Zhang Y, Li L, Yu R, et al. White matter integrity alterations in first episode, treatment-naive generalized anxiety disorder. *J Affect Disord*. 2013;148(2-3):196-201. doi:10.1016/j.jad.2012.11.060.
  35. Liao W, Xu Q, Mantini D, et al. Altered gray matter morphometry and resting-state functional and structural connectivity in social anxiety disorder. *Brain Res*. 2011;1388:167-177. doi:10.1016/j.brainres.2011.03.018.
  36. Tromp D. Calculate tract based weighted means. 2018:1-7. doi:10.22541/au.151794135.53105748.
  37. Nichols TE, Holmes AP. Nonparametric permutation tests for functional neuroimaging: A primer with examples. *Hum Brain Mapp*. 2002;15(1):1-25. doi:10.1002/hbm.1058.
  38. Winkler AM, Ridgway GR, Webster MA, Smith SM, Nichols TE. Permutation inference for the general linear model. *Neuroimage*. 2014;92:381-397. doi:10.1016/j.neuroimage.2014.01.060.
  39. Smith SM, Nichols TE. Threshold-free cluster enhancement: addressing problems of smoothing, threshold dependence and localisation in cluster inference. *Neuroimage*. 2009;44(1):83-98. doi:10.1016/j.neuroimage.2008.03.061.
  40. Seabold S, Perktold J. Statsmodels: econometric and statistical modeling with Python. In: *Proceedings of the 9th Python in Science Conference*. ; 2010:57-61.